Transactions of the 15th International Conference on
Structural Mechanics in Reactor Technology (SMiRT-15)
Seoul, Korea, August 15-20, 1999



# Dislocation Pileup Model for Back Stress Evolution in Crystalline Plasticity

Tadashi Hasebe and Yutaka Imaida

*Doshisha University, Japan*

ABSTRACT This paper proposes back stress evolution equation by introducing imaginary dislocation pileup model against representative cell wall as well as grain boundary within the framework of crystalline plasticity. The representative cell size is spontaneously evolved according to the evolution of drag stress where dislocation junction formation processes are taken into account. Strain history as well as strain rate effect on the Bauschinger effect and Hall–Petch relation are extensively discussed based on the polycrystal analyses.

## 1. INTRODUCTION

Recent developments in the gradient plasticity[1,2] have enabled us to introduce length–scale effects in the framework of the continuum theory of crystalline plasticity. In evaluating gradient terms quantitatively, however, spatial discretization, e.g., based on FEM, is inevitable, which leads us to considerable difficulties in direct modeling of the length–scales associated with evolutions of microstructures such as cell and subgrain having $\mu$m order. The Bauschinger effect, for example, which is an old example of the length–scale effects causing irreversibility of deformation, has been reported to be significantly microstructure dependent even for pure metals. This kind of dependency is mainly resulted from progressively evolving dislocation substructures during deformation, which cannot be directly dealt with by the gradient plasticity.

In the present paper, we propose a dislocation pileup model against global obstacles with two length scales, i.e, one being grain size order, the other cell or subgrain size order. Evolution equation of the back stress is developed based on the above model which can indirectly describe the "gradient effect" brought about by dislocation pileups at the microstructure order. Microscopic constitutive equation [3–5] applicable to a wide range of strain rates covering impact loading up to 10000/s is used as a framework. Also recovery processes during unloading and reverse loading is taken into account in the evolution equation by considering pair annihilations and rearrangement of dislocations. Effects of strain rate on the Bauschinger effect and Hall–Petch relation are extensively discussed based on the analyses for two kinds of FCC metals.

## 2. DRAG STRESS MODEL AND IMAGINARY CELL SIZE

### 2.1 *Drag Stress Evolution Equation*

This paper employs modified version of the evolution equation for the drag stress $K^{(\alpha)}$[5]. Basic formulation of the drag stress is the same as that in the previous paper [5] where forest intersections are considered to be responsible for strain history effect, i.e.,

$$K^{(\alpha)}=\sum_{\beta=1}^{N} Q_{\alpha\beta}g^{(\beta)}, \quad \dot{g}^{(\alpha)}=H(\gamma^{(\alpha)})|\dot{\gamma}^{(\alpha)}| \tag{1}$$

Here $Q_{\alpha\beta}$ is hardening ratio [3–5] and $g^{(\alpha)}$ represents self–hardening in the current state.

$H(\gamma^{(\alpha)})$ is the instantaneous hardening modulus, assumed to be given by,

$$H(\gamma^{(\alpha)})=h_0\left[\ (h_0/n\tau_0)\gamma^{(\alpha)}+1\ \right]^n \tag{2}$$

for pure metals. The evolution of the hardening ratio $Q_{\alpha\beta}$ represents evolution of microstructures like cell walls, which will act as global obstacles against mobile dislocations causing dislocation pileups. Using the interaction matrix $f_{\alpha\beta}$, which specifies the kinds of interactions between two dislocations [3-5], the hardening ratio $Q_{\alpha\beta}$ is defined here as,

$$Q_{\alpha\beta}=\delta_{\alpha\beta}+f_{\alpha\beta}S_{\alpha\beta} \tag{3}$$

where $S_{\alpha\beta}$ indicates strain history matrix having a form of,

$$S_{\alpha\beta}=\delta_{\alpha\beta}tanh\left[(W_p)_{\alpha\beta}/(W_p)_{sat}\right]\cdot\Gamma^{(\alpha)} \tag{4}$$

$(W_p)_{sat}$ is the plastic work in the saturated state and $\Gamma^{(\alpha)}$ shows apparent reduction of the strain history effect due to the inertial effect. The details of $\Gamma^{(\alpha)}$ is reported in the previous paper [5]. $(W_p)_{\alpha\beta}$ represents the plastic work for $\alpha$ slip system in correlation with $\beta$ slip system defined as,

$$(\dot{W}^p)_{\alpha\beta}\equiv C_{\alpha\beta}\dot{W}_p^{(\alpha)},\quad \dot{W}_p^{(\alpha)}=\tau^{(\alpha)}\dot{\gamma}^{(\alpha)} \tag{5}$$

We assume no interaction among active slip systems. Here $C_{\alpha\beta}$ shows the correlation coefficient representing activity of slip systems which takes 1 or 0 according to the activity/inactivity of the slip systems.

### 2.2 *Imaginary Cell Model and Representative Length*

This paper introduces a concept of "representative cell" possessing a representative length scale associated with evolved dislocation substructures. Here we postulate that the cell structures are evolved as a result of dislocation junction formations as schematically illustrated in Fig.1, which is closely related to the evolution of the drag stress defined above. Therefore we can assume that the imaginary cell size is given as a function of the reciprocal of the hardening ratio $Q_{\alpha\beta}$, e.g.,

$$d_{CELL}=f(Q_{mean})\equiv k/Q_{mean} \tag{6}$$

where $Q_{\mathrm{mean}}$ is given as a quadratic invariance of $Q_{\alpha\beta}$ as,

$$Q_{mean}\equiv\sqrt{Q_{\alpha\beta}Q_{\alpha\beta}/N} \tag{7}$$

In Eq.(6) $k$ is a constant being equal to $d_{GRAIN}$ when $d_{CELL}>d_{GRAIN}$, i.e., $Q_{\mathrm{mean}}=1$. Note that the representative cell size introduced above is not directly correspond to the actual cell size.

## 3. BACK STRESS MODEL

### 3.1 *Imaginary Dislocation Pileup model*

General form of the back stress evolution equation is assumed to be given by a summation of elastic and inelastic components as,

$$\dot{\Omega}^{(\alpha)}=(\dot{\Omega}^{(\alpha)})_E+(\dot{\Omega}^{(\alpha)})_{IN} \tag{8}$$

where $(\Omega^{(\alpha)})_E$, $(\Omega^{(\alpha)})_{IN}$ respectively express elastic and inelastic components. The elastic part shows evolution of internal elastic stress field developed by piled-up dislocations against global obstacles. The inelastic part, on the other hand, represents the other factors leading to irreversible processes such as inhomogeneous deformation within a grain supposed to be caused by constraints from surrounding grains together with lattice rotations. Here we ignore the contribution from the latter for simplicity and restrict our discussion to $(\Omega^{(\alpha)})_E$. The elastic component is further decomposed into two parts with different scale orders, i.e., (a)grain size order (10 to 100$\mu$m) and (b)cell or subgrain size order (a few $\mu$m). (a) is mainly responsible for Hall-Petch relation, while (b) for the Bauschinger effect.

We propose imaginary dislocation pileup model for the evolution of $(\Omega^{(\alpha)})_E$ by taking account of contributions from the above-mentioned two scales, i.e.,

$$(\dot{\Omega}^{(\alpha)})^E=c(\dot{\Omega}^{(\alpha)})^E_{GRAIN}+(1-c)(\dot{\Omega}^{(\alpha)})^E_{CELL} \tag{9}$$

where $c$ is a constant ranging from 0 to 1, which specifies contributions from grain boundary and cell wall to the back stress. The schematics of the imaginary dislocation pileup model is illustrated in Fig.2 for the case of (a). In general the grain size and its distribution can be externally given as initial conditions. The cell size, on the other hand, should be spontaneously introduced and evolved as the deformation proceeds according to Eq.(6) introduced above.

Consider a crystal grain with dislocation source at its center as illustrated in Fig.2, and assume one dimensional model where dislocations after reaching the boundary of the obstacle are successively accumulated. No interaction among slip systems is taken into account. The elastic stress field to be developed can be equated as,

$$(\Omega^{(\alpha)})^E_{OBS}=sgn(\tau^{(\alpha)})\frac{A_{OBS}}{<d^*_{OBS}-\bar{x}_N>+a}\cdot\left\langle 1-\frac{\left|(\Omega^{(\alpha)}_{t-\Delta t})^E_{OBS}\right|}{(\Omega^E)_{sat}}\right\rangle+\sum_{k=1}^{N-1}\frac{A_{OBS}}{a} \tag{10}$$

where $d_{OBS}\equiv 2d^*_{OBS}$ is the mean obstacle size, i.e., grain diameter for $OBS=GRAIN$ and cell size for $OBS=CELL$. $a$ is a cut-off distance. $N$ represents number of piled-up dislocations. $A_i$ is material constant with the order of $Gb/2\pi$ for $OBS=GRAIN$. We also assume that $N$th dislocation in motion is subject to back stress developed by already piled-up $N-1$ dislocations, and the elastic interaction between moving dislocations are neglected. Mean moving distance of dislocations $x$ is evaluated from the slip strain $\gamma^{(\alpha)}$ by multiplying a scale factor $l^*$, i.e.,

$$\bar{x}^{(\alpha)}=l^*\cdot\gamma^{(\alpha)} \tag{11}$$

The scale factor $l^*$ is formally given by $l^*=1/(\rho_m b)$ where $\rho_m$ and $b$ respectively are mobile dislocation density and the magnitude of Burgers vector, which can be derived from the well-known relation $\gamma=\rho_m bx$. $l^*$ is assumed to be constant though it is supposed to be strain rate dependent: $\rho_m$ is expected to become large under impact loading, for example, which makes $l^*$ smaller than that under static loading.

### 3.2 *Recovery Model For Unloading and Reverse Loading Processes*

Figure 3 schematically illustrates piling-up behavior of dislocations against cell wall during loading, unloading and reverse loading processes. Piled-up dislocations in the forward loading process are partially annihilated upon unloading due to pair annihilations. While these annihilation process proceeds, rearrangement of dislocation substructures occurs and pileups

at the other side of the cell wall proceeds. All of these processes will cause relaxation of the internal back stress field developed during the forward loading.

Recovery term becomes operative in unloading and reverse loading processes as,

$$\left(\Omega^{(\alpha)}\right)^{E+}_{CELL}=\left(\left(\Omega^{(\alpha)}\right)^{E+}_{CELL}\right)_{max}-g\left(\left|\left(\Omega^{(\alpha)}\right)^{E\pm}_{CELL}\right|,\ \dot{\gamma}^{(\alpha)}\right) \tag{12}$$

Here we simply assume that the recovery term is given by a power of the total internal stress, defined as a sum of absolute values of the back stresses from both sides of the obstacles, i.e.,

$$\begin{cases} \dot{g}=e\left|\left(\Omega^{(\alpha)}\right)^{E\pm}_{CELL}\right|^{m} \\ \left|\left(\Omega^{(\alpha)}\right)^{E\pm}_{CELL}\right|=\left|\left(\Omega^{(\alpha)}\right)^{E+}_{CELL}\right|+\left|\left(\Omega^{(\alpha)}\right)^{E-}_{CELL}\right| \end{cases} \tag{13}$$

where $e$ and $m$ are material constants being functions of stacking fault energy. For a material with large stacking fault energy, for example, $e$ takes large values leading to fast recovery.

## 4. MICROSCOPIC CONSTITUTIVE EQUATION

In this paper we use the following microscopic constitutive equation [1] as a framework which covers a wide range of strain rates up to $10^4 s^{-1}$.

$$\dot{\gamma}^{(\alpha)}=\dot{A}_{SR}\frac{\tau^{\alpha}-\Omega^{\alpha}}{K^{\alpha}}\left[\left|\frac{\tau^{(\alpha)}-\Omega^{(\alpha)}}{K^{(\alpha)}}\right|\exp B_{SR}\left(1.0-\left|\frac{\tau^{(\alpha)}-\Omega^{(\alpha)}}{K^{\alpha}}\right|\right)+C_{SR}\right]^{-1} \tag{14}$$

where $K^{(\alpha)}$ and $\Omega^{(\alpha)}$ are drag and back stress state variables, respectively, while $A_{sr}$, $B_{sr}$ and $C_{sr}$ are material constants. The constitutive equation has been derived [5] based on the dislocation dynamics [6] taking account of the two distinct activation mechanisms against dislocation motion [5,6], i.e., thermal activation mechanism for low and middle strain rates and phonon drag mechanism for high strain rates over $10^3 s^{-1}$. Figure 4 shows strain rate v.s. flow stress curve obtained based on Eq.(14) for Cu-type polycrystal, exhibiting the transition between the two mechanisms at around $10^3 s^{-1}$.

## 5. ANALYTICAL MODEL AND PROCEDURE

Polycrystal analyses with 800 grains based on the Taylor assumption are conducted for two types of FCC metals, i.e., Cu- and Al-types. The Cu-type is the representative of metals with low stacking fault energy (S.F.E.) while the Al-type that of high S.F.E. The former exhibits strong dislocation interaction in comparison with the latter.

Tension-compression analyses under static ($1\times10^{-3}s^{-3}$) and impact ($\sim5\times10^{3}s^{-3}$) loading conditions are made based on the proposed model to examine the effect of strain rate on the Bauschinger effect. The loading conditions are (1)static tension followed by static compression, (2)static tension followed by impact compression, and (3)impact tension followed by impact compression. The model is applied also to non-proportional cyclic loading to additionally discuss the representative cell size. Material parameters used in the present analyses are listed in Table 1.

## 6. ANALYTICAL RESULTS AND DISCUSSION

### 6.1 *Representative Cell Size Under Non-Proportional Loading*

Figure 5 shows variation of representative cell size $d_{CELL}$ with number of cycles under non-proportional cyclic strain paths. As clearly seen from the figure, $d_{CELL}$ decreases with increasing non-proportionality: a linear relationship is found between the reciprocal of $d_{CELL}$ and stress level as shown in Fig.6, which has been experimentally confirmed.

### 6.2 *Strain Rate Dependency of The Bauschinger Effect*

Figure 7 shows analytical result showing the Bauschinger effect (B.E.) under static loading condition (1) for Cu- and Al-types. Effect of pre-tension strain on the B.E. depending on material is clearly observed which qualitatively agrees with experimental results reported so far: large pre-strain effect for Cu and small pre-strain effect for Al. Figure 8 shows variation of the representative cell size $d_{CELL}$ during pre-tension for the two materials with increasing strain. The Cu-type yields rapid decrease of $d_{CELL}$ compared with the Al-type: this demonstrates that microstructure evolution significantly affects the B.E. Figure 9 shows effect of strain rate on the B.E for condition (2). The effect of pre-strain becomes large even for the Al-type. Figure 10 displays the B.E. under impact loading condition, i.e, (3). The B.E. becomes large as strain rate increases for both the materials. This trend comes from strain rate history effect: the drag stress evolves significantly under impact loading compares with static loading, which leads to decreasing size of the representative cell causing large B.E.

Figure 11 shows the effect of strain rate on the recovery process during unloading and reverse loading. For the static case, the recovery process is operative depending on the parameter $e$ in Eq.(15) while, for impact loading, there is almost no recovery. Figure 12 shows variation of the back stress during forward and reverse loading comparing the effect of strain rate. The results demonstrate very small recovery under impact reverse loading, also leading to large B.E. as in Fig.9.

### 6.3 *Hall-Petch Relation*

Figure 13 shows relationship between grain size and stress indicating the Hall-Petch (H.P.) relation for both the strain rates. There observed no strain rate effect on H.P. relation as far as the scale factor $l^*$ is set to be constant in the present analysis. Figure 14 shows effect of $l^*$ on the H.P. showing its strong dependency. As mentioned previously $l^*$ is considered to be a function of strain rate, so that the H.P. relation will also affected by strain rate, which should be confirmed by experiments.

## 7. CONCLUSION

(1)Back stress evolution equation is proposed considering imaginary dislocation pileup model where two scale orders are taken into account, i.e., cell and grain size orders.
(2)Strain rate effects on the Bauschinger effect, Hall-Petch relation are extensively discussed based on the analytical results.
(3)Variations of the representative cell size with strain history, strain rate and material are discussed in conjunction with the Bauschinger effect and additional hardening under non-proportional loading.

## REFERENCES

1. Zbib, H. M. & Aifantis, E. C. 1989, A Gradient-Dependent Flow Theory of Plasticity: Application to Metal and Soil Stabilities, *Appl. Mech. Rev.*, **42**, S295-S304.
2. Fleck, N. A. & Hutchinson, J. W. 1993, A Phenomenological Theory for Strain Gradient Effects in Plasticity, *J. Mech. Phys. Solids*, **41**, 1825-1857.
3. Hasebe, T., Y. Imaida, & H. Nakamoto 1995. Flow stress of FCC metals under unsteady transient loadings. *Dynamic Plasticity and Structural Behaviors (Proc. Plasticity '96)*, Osaka, Japan. 825-828. Gordon and Breach Publishers.
4. Hasebe, T., Y. Imaida, H. Nakamoto & K. Shibahara 1996. Strain rate and strain history effects on hardening behavior of FCC metals under dynamic loading -constitutive modelling based on the crystalline plasticity-. *Proc. AEPA '96*, Eds. T. Abe, T. Tsuta; 357-362. Pergamon.
5. Hasebe, T., Y. Imaida 1997. Modelling of Strain Rate-Strain History Coupling Effect. *Proc. SMiRT 14*, **9** (*Division L*), 13-20.
6. Meyers, M. A. 1994, Dynamic Behavior of Materials, John Wiley & Sons.

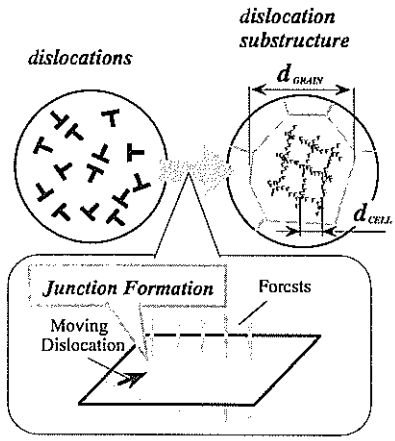


Fig.1 Basic concept of evolution model for dislocation substructures as a result of junction formation.

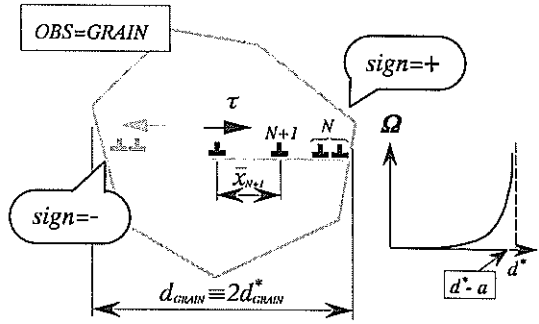


Fig.2 Schematics of dislocation pile-up model for back stres s evolution for *OBS=GRAIN*.

Table 1 Material parameters employed in the analysis.

| | Cu-type | Al-type |
|---|---|---|
| $c_{11}$ | 168400 [MPa] | 108200 [MPa] |
| $c_{12}$ | 121400 [MPa] | 61300 [MPa] |
| $c_{44}$ | 75400 [MPa] | 28500 [MPa] |
| $\tau_0$ | 35 | 18 |
| $h_0$ | $1.5\times10^5$ | $7.0\times10^4$ |
| $n$ | 0.35 | 0.3 |
| $A_\sigma$ | 0.8 | 0.5 |
| $B_\sigma$ | 20 | 30 |
| $C_\sigma$ | $5.3\times10^{-4}$ | $2.0\times10^{-4}$ |
| $f_{opt}$ 0 | 0.0 | 0.0 |
| $f_{opt}$ N | 0.0 | 0.0 |
| $f_{opt}$ C | 0.0 | 0.0 |
| $f_{opt}$ H | 2.0 | 0.5 |
| $f_{opt}$ G | 4.0 | 1.0 |
| $f_{opt}$ S | 6.0 | 1.5 |

| | Cu-type | Al-type |
|---|---|---|
| $(W_p)_{sat}$ | 100 | 8 |
| $\xi_\sigma$ | $1.0\times10^5$ | 1.8 |
| $\xi_h$ | 0 | 0 |
| $P_1$ | 1.0 | 1.0 |
| $P_2$ | 1.0 | 1.0 |
| $d_{GRAIN}$ | 28 [μm] | 28 [μm] |
| $l^*$ | 18 | 31 |
| $A_{GRAIN}$ | $1.0\times10^{-3}$ | $3.0\times10^{-4}$ |
| $A_{CELL}$ | $1.0\times10^{-5}$ | $3.0\times10^{-6}$ |
| $(\Omega^*)_{sat}$ | 55 | 15 |
| $a^*$ | 0.1 | 0.1 |
| $c$ | 0.5 | 0.5 |
| $k$ | $1.0\times10^{-3}$ | $3.5\times10^{-3}$ |
| $e$ | 0.1 | 0.5 |
| $m$ | 0.3 | 0.5 |

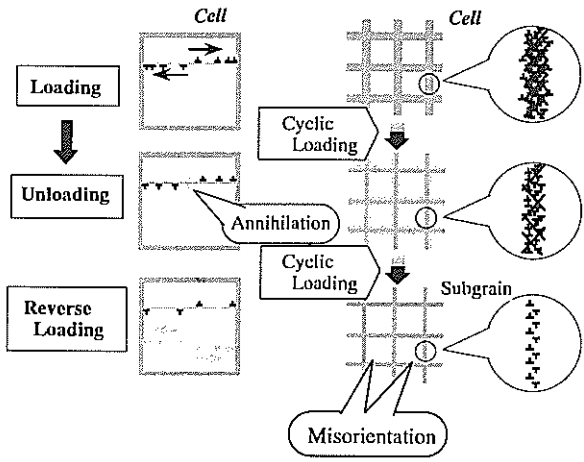


Fig.3 Behavior of pile-up dislocations against cell wall and schematics of recovery processes during unloading and reverse loading.

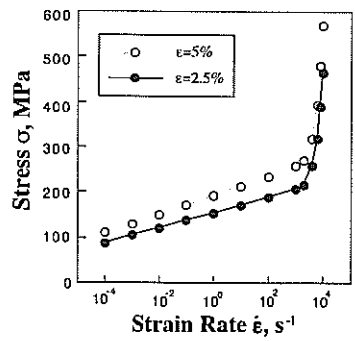


Fig.4 Strain rate v.s. flow stress obtained in analysis showing transition ofstrain rate sensitivity at aruund 5000/s.

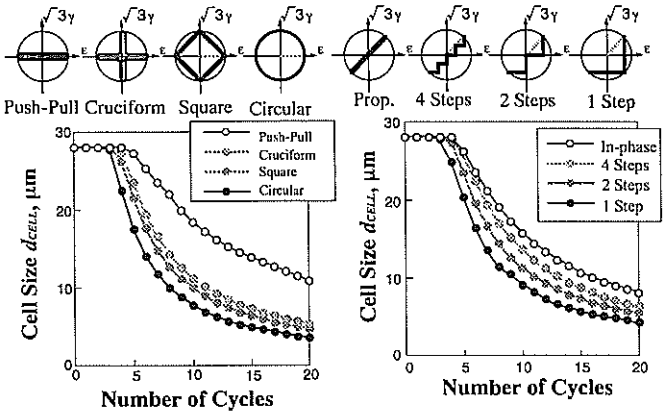


Fig.5 Variation of cell size with straining cycles comparing non-proportional strain paths.

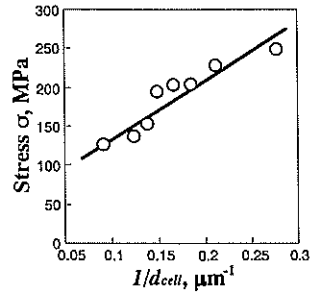


Fig.6 Relationship between inverse of cell size and stress for non-proportional strain paths.

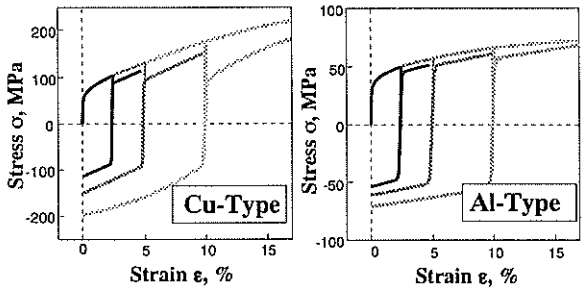


Fig.7 Stress response under tension-compression loading comparing effect of pre-strain on the Bauschinger effect.

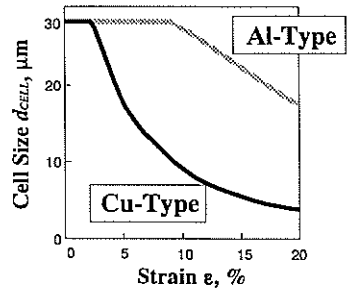


Fig.8 Variation of cell size with strain under monotonic tension comparing Al- and Cu-types.

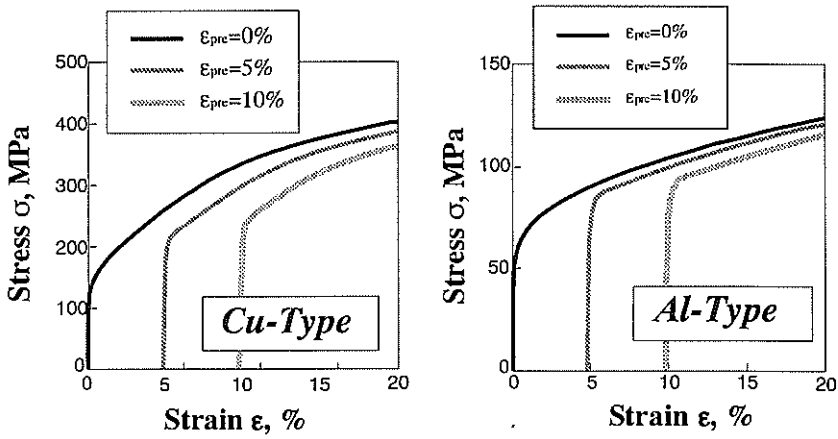


Fig.9 Bauchinger effect under impact compression following static pre-tension.

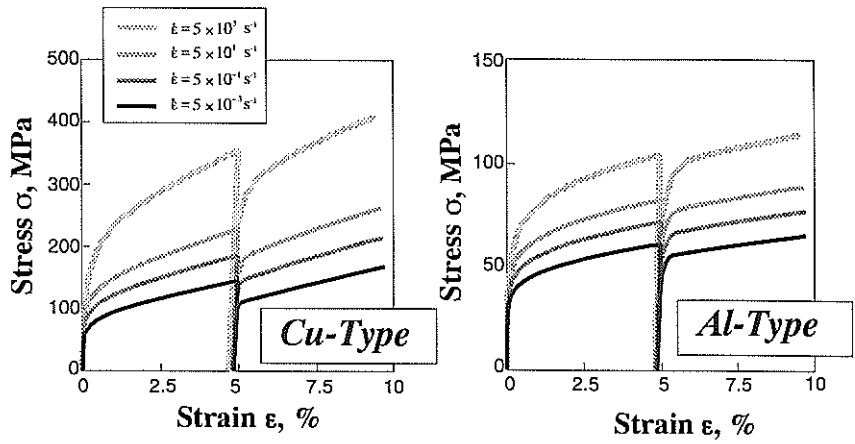


Fig.10 Effect of strain rate on the Bauschinger effect.

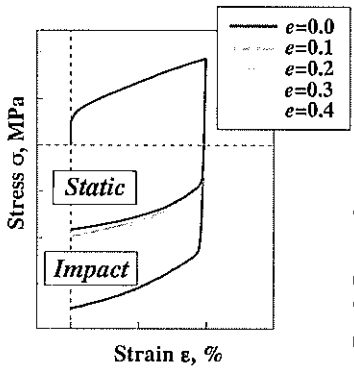


Fig.11 Effect of recovery term in the back stress model on Bauschinger behavior for static andimpact compressioo following static pre-tension.

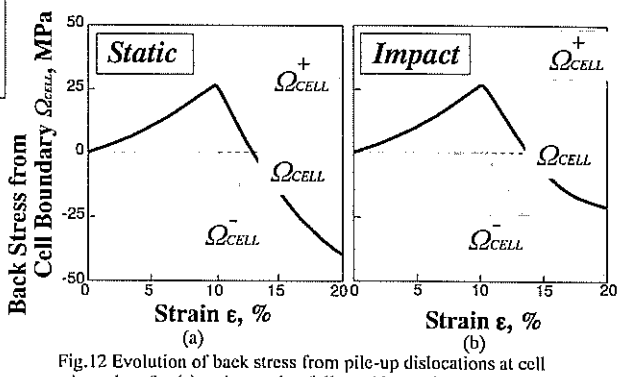


Fig.12 Evolution of back stress from pile-up dislocations at cell boundary for (a)static tension followed by static compression and (b) static tension followed by impact compression.

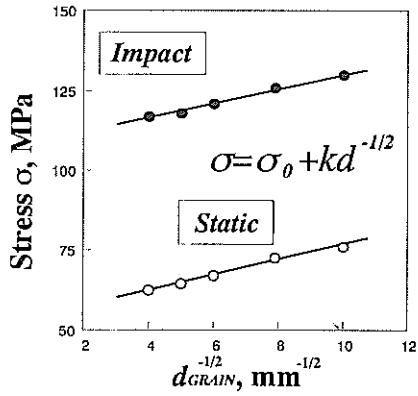


Fig.13 Flow stress as a function of grain size parameter showing Hall-Petch relation under static and impact tension.

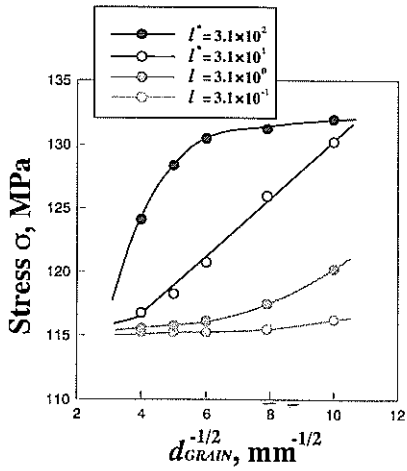


Fig.14 Analytical result showing effect of scale parameter $l^*$ on Hall-Petch relation.